Stem Cell Reports
Report
ISSCR
OPEN ACCESS

CHD4 ensures stem cell lineage fidelity during skeletal muscle regeneration

Krishnamoorthy Sreenivasan,[1,11] Alejandra Rodríguez-delaRosa,[2,11] Johnny Kim,[1,3] Diana Mesquita,[2] Jessica Segalés,[2] Pablo Gómez-del Arco,[4,5] Isabel Espejo,[6] Alessandro Ianni,[1] Luciano Di Croce,[6,1,7] Frederic Relaix,[8] Juan Miguel Redondo,[5] Thomas Braun,[1,3,9] Antonio L. Serrano,[2,*] Eusebio Perdiguero,[2,*] and Pura Muñoz-Cánoves[2,7,10,*]

[1]Department of Cardiac Development and Remodeling, Max Planck Institute for Heart and Lung Research, Bad Nauheim, Germany
[2]Department of Experimental & Health Sciences, University Pompeu Fabra (UPF), CIBERNED, 08003 Barcelona, Spain
[3]German Center for Cardiovascular Research (DZHK), Rhine Main, Germany
[4]Institute of Rare Diseases Research, Instituto de Salud Carlos III (ISCIII), 28220 Majadahonda, Madrid, Spain
[5]Gene Regulation in Cardiovascular Remodelling & Inflammation Laboratory, Centro Nacional de Investigaciones Cardiovasculares Carlos III (CNIC), 28029 Madrid, Spain
[6]Centre for Genomic Regulation (CRG), Barcelona Institute of Science and Technology, Barcelona, 08003 Barcelona, Spain
[7]ICREA, 08010 Barcelona, Spain
[8]Univ Paris Est Creteil, INSERM, EnvA, EFS, AP-HP, IMRB, F-94010 Creteil, France
[9]German Center for Lung Research (DZL), Giessen, Germany
[10]Centro Nacional de Investigaciones Cardiovasculares (CNIC), 28029 Madrid, Spain
[11]Co-first author
*Correspondence: antonio.serrano@upf.edu (A.L.S.), eusebio.perdiguero@upf.edu (E.P.), pura.munoz@upf.edu (P.M.-C.)
https://doi.org/10.1016/j.stemcr.2021.07.022

SUMMARY

Regeneration of skeletal muscle requires resident stem cells called satellite cells. Here, we report that the chromatin remodeler CHD4, a member of the nucleosome remodeling and deacetylase (NuRD) repressive complex, is essential for the expansion and regenerative functions of satellite cells. We show that conditional deletion of the *Chd4* gene in satellite cells results in failure to regenerate muscle after injury. This defect is principally associated with increased stem cell plasticity and lineage infidelity during the expansion of satellite cells, caused by de-repression of non-muscle-cell lineage genes in the absence of *Chd4*. Thus, CHD4 ensures that a transcriptional program that safeguards satellite cell identity during muscle regeneration is maintained. Given the therapeutic potential of muscle stem cells in diverse neuromuscular pathologies, CHD4 constitutes an attractive target for satellite cell-based therapies.

INTRODUCTION

Adult skeletal muscles regenerate through a population of muscle-resident *Pax7*-expressing stem cells (satellite cells [SCs]) that are quiescent in resting conditions. Upon injury, SCs exit quiescence and proliferate, and their progeny either differentiate to form new muscle fibers or self-renew to replenish the quiescent stem cell pool (Yin et al., 2013). SC fate is controlled by an interplay of instructive and responsive cues, which are epigenetically regulated at a cell-autonomous level (Ermolaeva et al., 2018; Faralli et al., 2016; Juan et al., 2011; Robinson and Dilworth, 2018; Schworer et al., 2016; Zhang et al., 2015).

The chromatin-remodeling complex NuRD (nucleosome remodeling and deacetylase) is an epigenetic regulator implicated in various cellular processes, such as cell-cycle progression, DNA damage response, maintenance of genome integrity, lineage commitment of different cell types (including stem cells), and proliferation of cancer cells (Gomez-del Arco et al., 2016; Kashiwagi et al., 2007; Lai and Wade, 2011; O'Shaughnessy and Hendrich, 2013; Ostapcuk et al., 2018; Williams et al., 2004; Xu et al., 2020; Zhang et al., 1998; Zhao et al., 2017). Different NuRD complexes with a diverse assembly of protein components yield distinct outcomes, including transcriptional activation or repression of target genes. These components include the chromodomain-helicase-DNA-binding proteins 3 and 4 (CHD3, CHD4), which both possess helicase/ATPase activity, the class I histone deacetylases 1 and 2 (HDAC1 and HDAC2), the metastasis-associated proteins Mta1/2/3, and the methyl-CpG-binding domain family members MBD2 or MBD3. These core factors can assemble into mutually exclusive CHD4/NuRD-like complexes (Le Guezennec et al., 2006). We previously demonstrated that *Chd4* maintains tissue homeostasis and identity of mature cardiac and skeletal muscle (Gomez-del Arco et al., 2016) and plays a decisive role in the de-repression of RIPK3, a key effector of necroptosis (Sreenivasan et al., 2020).

Here, we show that CHD4 is not only an essential component of the muscle regenerative program that sustains efficient expansion of adult muscle stem cells but it is also required to maintain their transcriptional identity.

RESULTS

CHD4 expression in SCs is required for muscle regeneration

We first assessed *Chd4* expression in quiescent SCs (QSCs) isolated from resting muscle of wild-type (WT)

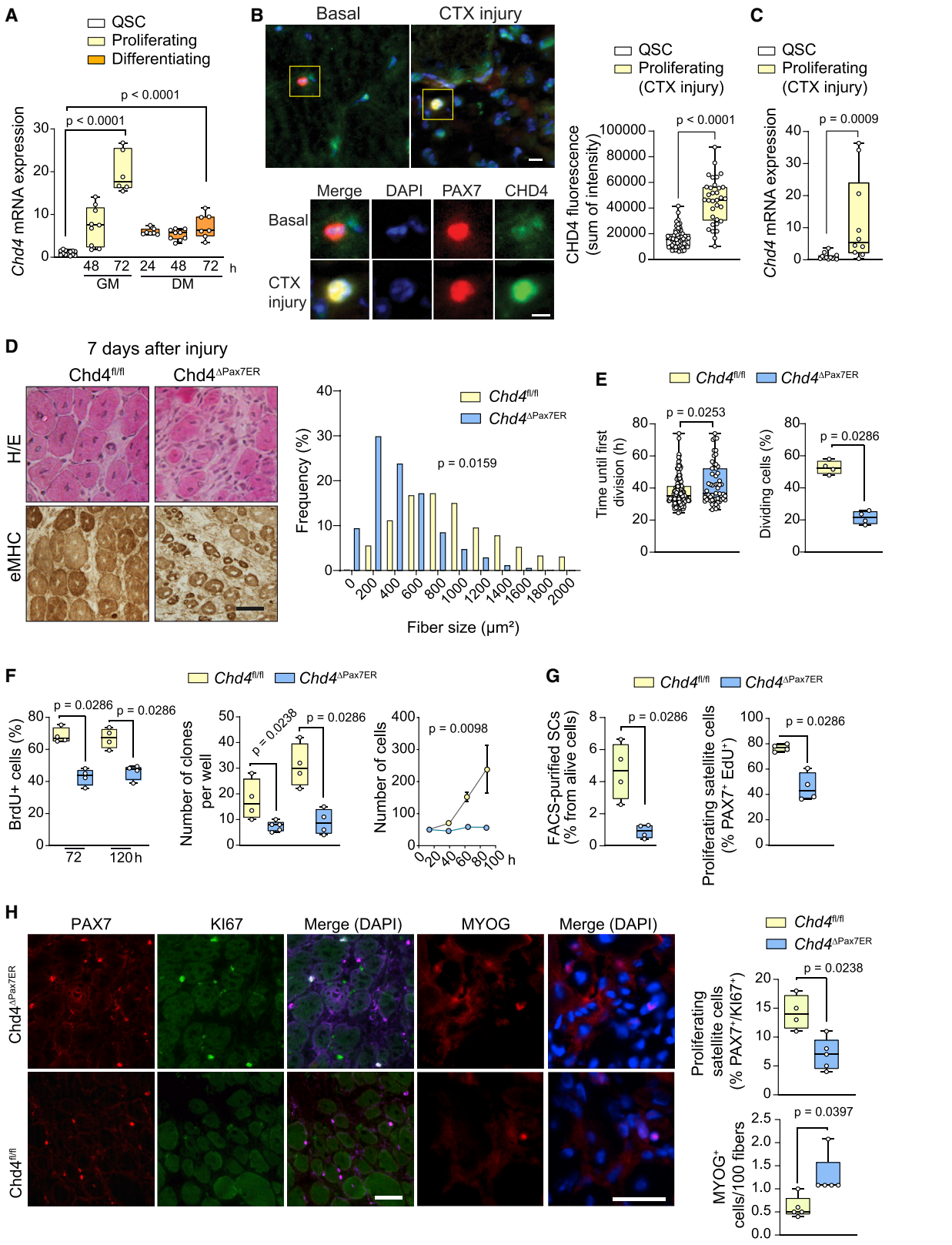

(legend on next page)

mice using a α7-integrin$^+$/CD34$^+$/SCA1$^-$/CD45$^-$ fluorescence-activated cell sorting (FACS) protocol and cultured in growth medium for 48/72 h, or differentiation medium for 24/48/72 h. *Chd4* mRNA expression was upregulated in proliferating SCs, decreasing during early differentiation stages (Figure 1A). Consistently, in SCs isolated from regenerating muscle 72 h after injury, the peak of the proliferative response, *Chd4* expression was strongly induced (Figure 1B) at both transcript and protein levels (Figure 1C).

To assess the specific contribution of Chd4 to SC functions, we generated mice with conditional deletion of *Chd4* in SCs (*Chd4*$^{\Delta Pax7ER}$ mice) by intercrossing *Chd4*$^{fl/fl}$ and *Pax7*$^{CRE\text{-}ER}$ mice (Nishijo et al., 2009; Williams et al., 2004). Loss of *Chd4* after tamoxifen (TMX) administration was verified by RT-PCR (Figure S1A). In the absence of injury, muscles of *Chd4*$^{\Delta Pax7ER}$ and *Chd4*$^{f/fl}$ (control) mice showed no significant differences in muscle morphology (Figure S1B), and the number of Pax7$^+$ cells was similar, with a tendency to decrease by 90 days after TMX administration (Figure S1C). At 7 days after injury, muscle regeneration in *Chd4*$^{\Delta Pax7ER}$ mice was severely impaired, as indexed by the reduced size of myofibers positive for embryonic myosin heavy chain (eMHC), a marker of newly formed myofibers (Figure 1D). The muscles of *Chd4*$^{\Delta Pax7ER}$ mice continued to show smaller eMHC$^+$ and centrally nucleated fibers (indicative of regeneration) than control mice at 14 or 21 days after injury (Figures S1D and S1E). This persistent regenerative defect in *Chd4*$^{\Delta Pax7ER}$ mice was exacerbated after two rounds of muscle injury (Figure S1F).

CHD4 is essential for efficient SC proliferation during muscle regeneration

We next determined myogenic functions of SCs upon quiescence exit. Compared with *Chd4*$^{fl/fl}$, *Chd4*$^{\Delta Pax7ER}$ SCs exhibit proliferation arrest as revealed by live time-lapse microscopy (Figure 1E), 5-bromo-2′-deoxyuridine (BrdU) incorporation in growth-promoting conditions (Figure 1F), and clonogenic assays (Figure 1F). Importantly, acute *Chd4* deletion *ex vivo* by adenovirus-CRE (Ad-CRE, compared with Ad-GFP) in SCs isolated from *Chd4*$^{fl/fl}$ mice (Figure S1G) induced a proliferation arrest, thereby excluding potential indirect effects of long-term TMX-mediated *Chd4* deletion (Figure S1G).

Consistently, compared with *Chd4*$^{fl/fl}$, the total number and fraction of proliferating (PAX7$^+$/EdU$^+$ or PAX7$^+$/KI67$^+$) SCs from regenerating muscles *in vivo* were dramatically lower in *Chd4*$^{\Delta Pax7ER}$ mice (Figures 1G and 1H), coinciding with an increased number of differentiating (Myogenin, Myog$^+$) SCs (Figure 1H), and a reduced proportion of self-renewed SCs (Figure S1H). Consistently, impairment of self-renewal and regeneration in *Chd4*$^{\Delta Pax7ER}$ mice was exacerbated upon repetitive injuries (Figure S1F). Furthermore, regenerating myofibers in *Chd4*$^{\Delta Pax7ER}$ mice contained significantly fewer myonuclei (Figure S1I), a feature also observed in *in vitro*-formed myotubes (Figure S1J).

To obtain a molecular understanding of how *Chd4* affects SC proliferation, we performed whole-transcriptome analyses of *Chd4*$^{fl/fl}$ SCs cultured in growth medium for 72 h with acute Ad-CRE-mediated deletion of *Chd4*, resulting in the upregulation of 1,975 genes, and the downregulation of 1,843 genes (adjusted $p < 0.01$), compared with Ad-GFP transduced controls (Figure 2A). The upregulated

Figure 1. *Chd4* is required for the proliferative expansion of SCs during muscle regeneration

(A) *Chd4* mRNA relative expression in QSCs, and in SCs under proliferative (in growth medium [GM]) or differentiation (in differentiation medium [DM]) conditions at the indicated time points in culture from WT mice. Data were normalized to housekeeping gene *Rpl7* with the QSCs set to 1 (from left to right, n = 13, 9, 6, 7, 9, or 7 mice, respectively).

(B) Representative pictures and quantification of Chd4 in SCs (Pax7$^+$) from non-injured muscles from WT mice, or at 72 h after muscle injury with CTX (n = 33 or 60 cells, respectively, from four mice). The sum of the Chd4 fluorescence intensity per cell is represented. Scale bar, 5 μm.

(C) *Chd4* mRNA expression in freshly isolated SCs from non-injured muscles and at 72 h after muscle injury with CTX. Data were normalized to housekeeping gene *Rpl7*, with the QSCs set to 1 (n = 12 or 9 mice, respectively).

(D) Representative pictures of sections of regenerating muscles from TMX-treated *Chd4*$^{fl/f}$ and *Chd4*$^{\Delta Pax7ER}$ mice at day 7 after injury, stained with hematoxylin and eosin and antibodies against eMHC. Scale bar, 10 μm (top), 5 μm (bottom). Frequency distribution of cross-sectional area (μm^2) of regenerating fibers from TMX-treated *Chd4*$^{fl/f}$ and *Chd4*$^{\Delta Pax7ER}$ mice (n = 4 and 5 mice, respectively) (bottom).

(E) Average time until first division during live time-lapse microscopy, and percentage of dividing SCs from TMX-treated *Chd4*$^{fl/f}$ and *Chd4*$^{\Delta Pax7ER}$ mice (138 or 58 individual cells from three different mice, respectively).

(F) Percentage of BrdU$^+$ SCs cultured in GM for either 72 or 120 h (left), the number of SC colonies with more than five cells counted throughout 4 days after isolation and culture in GM (middle), and the number of SCs per well after seeding 50 cells/well at time 0 (right), from TMX-treated *Chd4*$^{fl/f}$ and *Chd4*$^{\Delta Pax7ER}$ mice (n = 4 independent experiments).

(G) Relative number of total and proliferating SCs after FACS purification from TMX-treated *Chd4*$^{fl/f}$ or *Chd4*$^{\Delta Pax7ER}$ mice at 3 days after injury (n = 4 mice/group).

(H) Representative pictures and quantification of proliferating (Pax7$^+$/Ki67$^+$; n = 4 mice/group) or differentiating cells (Myog; n = 5 mice/group) in muscles of TMX-treated *Chd4*$^{fl/f}$ or *Chd4*$^{\Delta Pax7ER}$ mice at 7 days after injury. Scale bar, 50 μm.

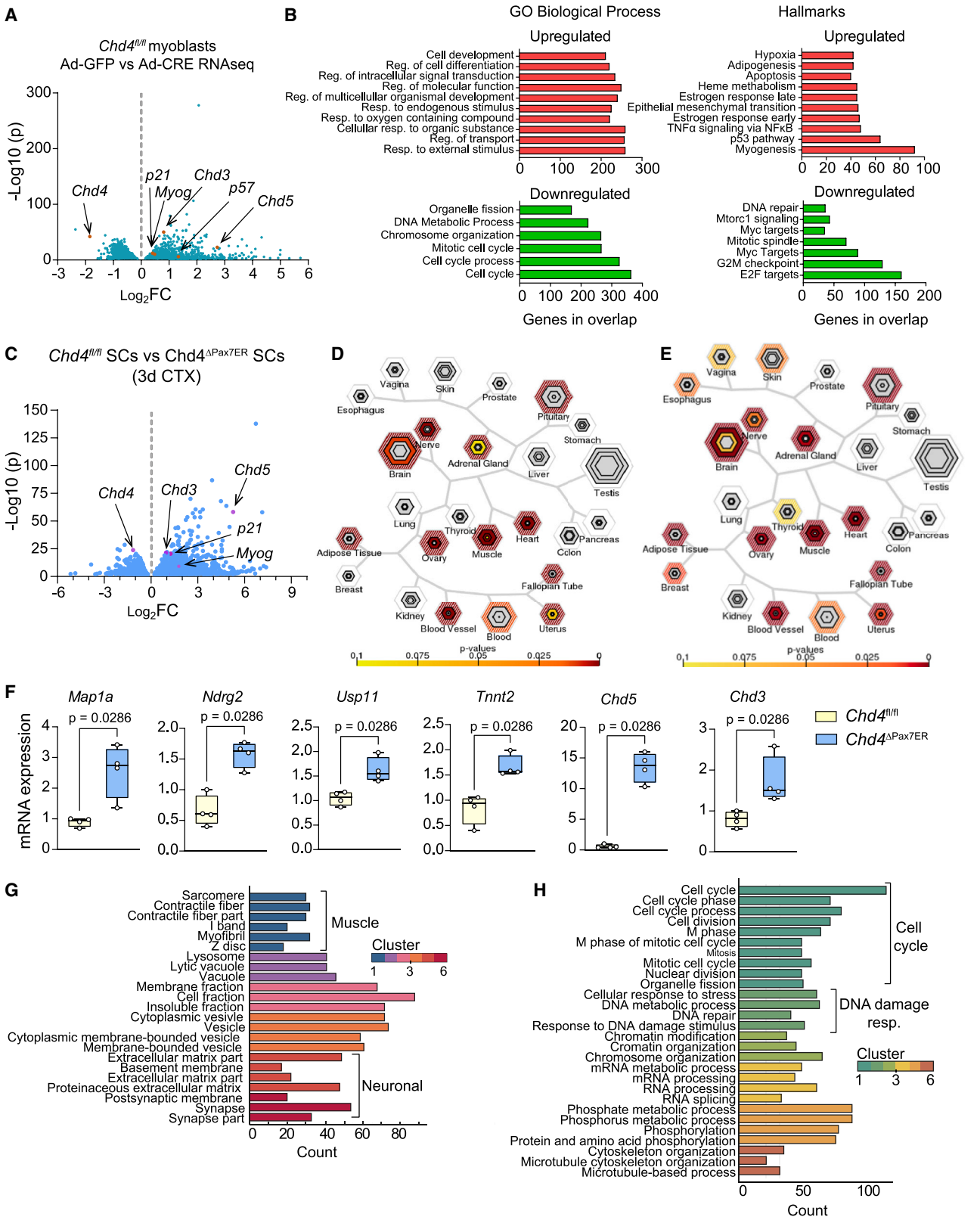

(legend on next page)

genes included the *Chd4* homologs *Chd3* and *Chd5*, suggesting a rapid compensatory attempt to uphold the availability of an alternative NuRD complex. Upregulated gene clusters were involved in cell differentiation toward myogenesis but also other cell lineages, and downregulated gene clusters were involved in cell-cycle and DNA metabolism processes (Figure 2B). Within the upregulated genes, we found increased *Myog* expression, a member of the myogenic regulatory factor (MRF) family required for muscle-cell differentiation (Figures 2A and S2A), and of *Cdkn1c* (*p57*) (Figures 2A and S2B), which has been linked to cell-cycle arrest and is required for the initiation of muscle differentiation (Mademtzoglou et al., 2018; Zhang et al., 1999). In agreement, we confirmed an upregulation of *p57* and *Myog* in SCs isolated from regenerating muscles of $Chd4^{\Delta Pax7ER}$ mice after injury (Figures S2A and S2B).

We next investigated *Chd4* regulation of *p57* due to its important role in regulating growth arrest of adult SCs. CHD4 chromatin immunoprecipitation (ChIP) followed by PCR revealed a direct association to the *p57* gene regulatory regions in proliferating SCs (Figure S2C). In agreement with this, lentivirus-mediated knockdown of *p57* increased SC proliferation (Figure S2D). To determine the influence of the upregulated *p57* expression in SCs of $Chd4^{\Delta Pax7ER}$ mice *in vivo*, we used a p57 conditional-mutant allele (Mademtzoglou et al., 2017) to generate $Chd4^{\Delta Pax7ER}$;$p57^{\Delta Pax7ER}$ double-mutant mice. Genetic inactivation of *p57* in *Chd4*-deficient SCs failed to restore SC proliferation or normal muscle regeneration (Figure S2E), and also did not affect the dysregulation of genes from other lineages *in vivo* (Figure S2F), showing that CHD4 controls SC function through the concurrent regulation of several target genes with distinct biological functions.

CHD4 maintains the transcriptional identity of SCs during muscle regeneration

To gain a deeper mechanistic understanding of the action of CHD4 in SCs *in vivo*, we performed RNA sequencing (RNA-seq) and transposase-accessible chromatin high-throughput sequencing (ATAC-seq) on SCs isolated from TMX-treated $Chd4^{fl/fl}$ and $Chd4^{\Delta Pax7ER}$ mice 3 days post injury. RNA-seq analysis identified 1,721 significantly upregulated genes and 1,226 significantly downregulated genes in $Chd4^{\Delta Pax7ER}$ SCs (Figures 2C), 41% and 47% of which were similarly up- or downregulated *in vitro* (Figure S2G). In agreement with our previous report, *Chd4* loss upregulated *Ripk3* (Sreenivasan et al., 2020). Furthermore, comparison of the *in vitro* and *in vivo* RNA-seq data confirmed increased expression of *p21*, a trend toward *p57* upregulation, as well as increased expression of the MRFs *MyoD* and *Myog*, involved in SC proliferation and early differentiation, and of genes specific to mature skeletal muscle (Figures 2D and 2E). Notably, tissue specific expression analysis (TSEA) further revealed upregulation of genes not related to the skeletal muscle lineage, including brain-related genes such as *Map1a*, *Nrdg2*, and *Usp11*, and heart-related genes such as cardiac troponin T (*Tnnt2*), which were confirmed by qRT-PCR (Figures 2F and S2H). These observations, together with clustering of altered Gene Ontology (GO) biological process categories via using the database for annotation, visualization and integrated discovery (DAVID) (Figure 2G), strongly indicate that SCs require *Chd4* to retain muscle stem cell identity in regenerating muscles, especially during the proliferative phase after injury.

RNA-seq of *Chd4*-deficient SCs *in vivo* also identified the downregulation of two important gene clusters: one involved in positive regulation of the cell cycle (e.g., cyclin-dependent kinase 4 [*Cdk4*]), and one in DNA damage repair (e.g., replication protein A1 [*Rpa1*]); these may contribute to the observed proliferative phenotype (Figure 2H). $Chd4^{\Delta Pax7ER}$ SCs also showed changes in the expression of other NuRD complex subunits (e.g., histone deacetylase 1 [*Hdac1*]), other CHD family genes (e.g., chromodomain helicase DNA-binding protein 5 [*Chd5*]), histone variants (e.g., histone cluster 1 H1 family member C [*Hist1h1c*]), and some Polycomb repressive complex 2 (PRC2) components (e.g., enhancer of zeste 2 [*Ezh2*]) (Figure S3A). These changes are particularly important, pointing to the consequent complexity of dysregulated epigenetic repression occurring in the absence of *Chd4*,

Figure 2. *Chd4* controls the expression of cell-cycle regulators and lineage-specific genes in SCs

(A) Volcano plot ($-\log_{10}$(p) versus $\log_2$(fold change)) showing RNA-seq results from $Chd4^{fl/fl}$ SCs transduced with Ad-CRE or Ad-GFP (control) (n = 4 independent experiments).

(B) GO analysis of the Biological Process database and Hallmark database of the significantly upregulated and downregulated genes.

(C) Volcano plot showing RNA-seq results from FACS-purified SCs at 3 days after TMX-induced muscle injury, in $Chd4^{fl/fl}$ and $Chd4^{\Delta Pax7ER}$ mice (n = 4 mice/group).

(D) TSEA analyses comparing gene expression of $Chd4^{fl/fl}$ SCs transduced with Ad-CRE or Ad-GFP.

(E) TSEA analyses of gene expression from SCs purified from TMX-treated $Chd4^{fl/fl}$ or $Chd4^{\Delta Pax7ER}$ mice at 3 days after muscle injury.

(F) Relative mRNA expression of the indicated genes in $Chd4^{fl/f}$ or $Chd4^{\Delta Pax7ER}$ mice SCs at 3 days after injury (n = 4 mice/group). Data were normalized to housekeeping gene *Rpl7*, with the $Chd4^{fl/f}$ set to 1.

(G and H) Functional annotation clustering based on DAVID biological processes of upregulated genes (G) or downregulated genes (H) in FACS-purified SCs, as in (C).

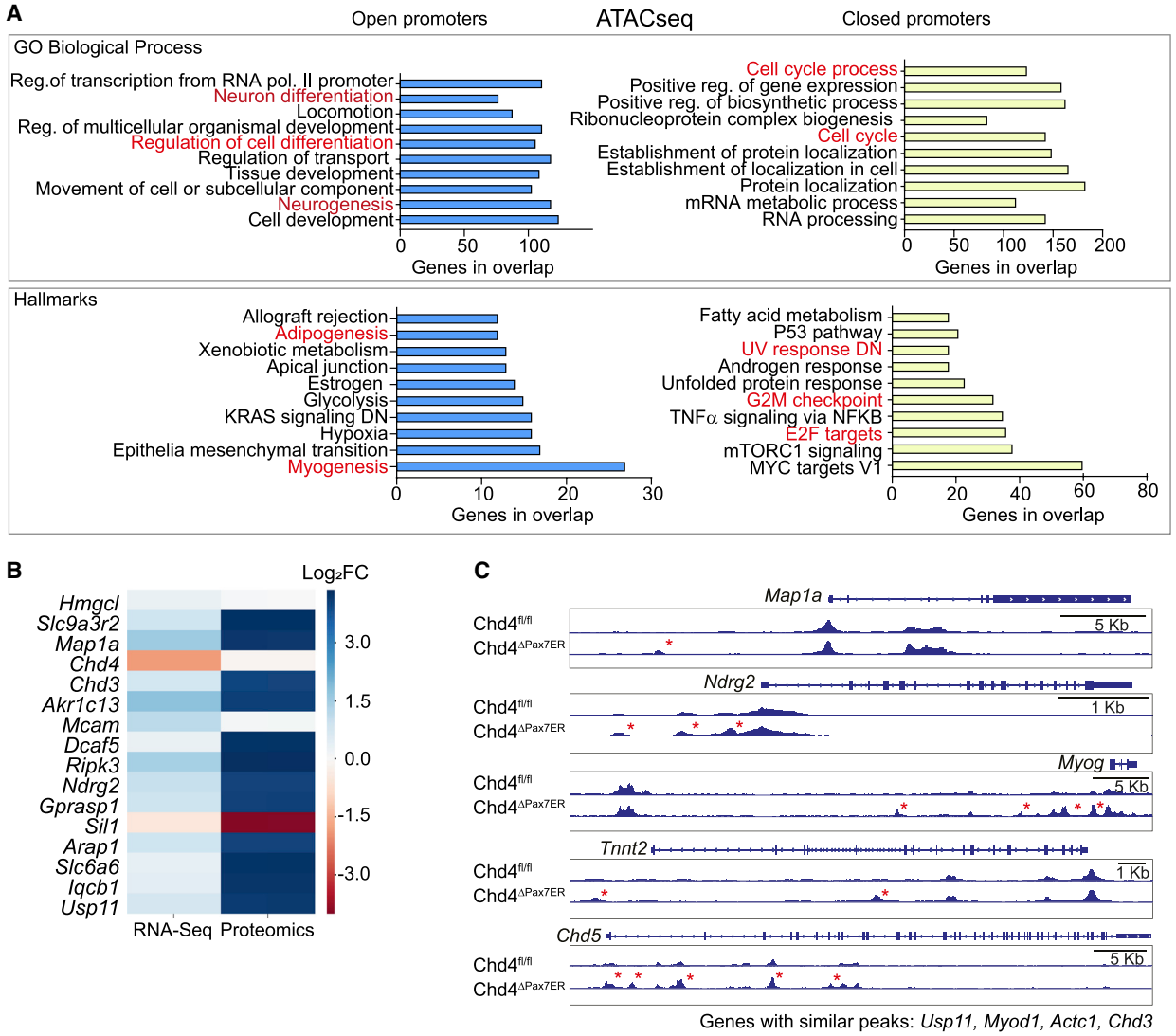

(legend on next page)

and thereby providing a potential explanation for the expression of genes from diverse lineages.

Supporting the transcriptomic data, ATAC-seq analysis of *Chd4*-deficient cells sorted 3 days after muscle injury showed extensive changes in proximal promoters near transcriptional start sites (TSSs), with 1,600 peaks significantly more open (e.g., with more accessible chromatin) and 1,436 significantly more closed. GO analysis of these changed genes revealed similar categories to those found by RNA-seq. For instance, myogenesis and neuronal differentiation gene promoters were significantly more open, whereas cell-cycle regulation, G2/M checkpoint, and E2F-regulated proliferation-related gene promoters were significantly more closed (Figure 3A).

Integration of proteomic and transcriptomic analyses of *Chd4*-deficient SCs (Sreenivasan et al., 2020), identified 18 commonly upregulated or downregulated proteins, including CHD3 and the neural proteins NDRG2, USP11, and MAP1a (Figure 3B). More importantly, $Chd4^{\Delta Pax7ER}$ SCs displayed inappropriate accessibility of lineage genes including *Map1a*, *Ndrg2*, *Myog*, *Tnnt2*, and *Chd5* (Figure 3C). CHD4 binding to these loci was confirmed by ChIP-qPCR (Figure 3D), indicating direct repression.

CHD4 functions in SCs are intrinsic to the NuRD complex

We analyzed the interaction of other core NuRD subunits (MTA1 and HDAC1) in the absence of *Chd4*. Interestingly, the binding of MTA1 to HDAC1 was significantly reduced but not completely abolished (Figure S3B), indicating that CHD4 functions to promote the association of the NuRD complex to cognate binding sites in SCs. In agreement with this, histone acetylation was increased at the promoters of *Chd4*-regulated genes (Figure S3C), indicating reduced HDAC activity of the CHD4/NuRD complex in those promoters. ChIP-PCR analysis of HDAC1 on its cardinal target *p21* gene locus (Mal et al., 2001) showed that the absence of *Chd4* impaired HDAC1 recruitment (Figure S3D). Consistently, inhibition of HDAC1 in WT cells with romidepsin (Furumai et al., 2002) induced upregulation of the *Map1a* and *Ndrg2* genes, similarly to *Chd4* loss (Figure S3E).

As *Chd4* deletion upregulated the expression of *Chd3*, we asked if an alternate CHD3/NuRD complex exists and, if so, whether it could act redundantly. Notably, *Chd3* knockdown reduced the expression of *Chd4*, and vice versa (Figure S3F), pointing to a cross-regulation of both genes in SCs. Knockdown of either *Chd3* or *Chd4* resulted in a similar reduction of SC proliferation (Figures 1E–1G and S3F). Interestingly, the reduction of SC proliferation by single knockdown of *Chd4* or *Chd3* was not increased upon knockdown of both *Chd4* and *Chd3* (Figure S3F). These results show that CHD4's actions in SCs are integral to the NuRD complex and that the CHD4 and CHD3 complexes may be present in SCs with overlapping functionalities.

DISCUSSION

This study dissects novel functional roles of the epigenetic modifier CHD4 in SCs during skeletal muscle regeneration, including cell identity and cellular expansion. Our results revealed that *Chd4* loss breaks satellite lineage confinement and allows the expression of genes associated with other fates, indicating that its function is required for strict control of muscle lineage plasticity during regeneration.

In support of this notion, *Chd4* loss induced upregulation of genes corresponding to multiple lineages in proliferating SCs, both *in vitro* and during muscle regeneration, including the brain and neural proteins NDGR2, USP11, and MAP1A at both the transcript and the protein level. Notably, *Chd4* depletion also triggered the upregulation of *Chd5*, which encodes a neural-specific chromatin remodeler in the same CHD family as CHD3 and CHD4. CHD5 activates neuronal genes required for terminal neuronal differentiation (Egan et al., 2013; Potts et al., 2011). Therefore, it is tempting to speculate that CHD5 could be responsible for de-repression of neural genes, in an NuRD-dependent or -independent manner. Also, *Chd4* loss significantly upregulated the expression of cardiac-specific genes, in agreement with our previous studies showing inappropriate expression of cardiac sarcomeric genes in *Chd4*-deficient mature

Figure 3. Chd4 maintains the transcriptional identity of SCs during muscle regeneration

(A) GO analysis of the genes with differential open (left) and closed (right) chromatin from SCs obtained from TMX-treated $Chd4^{fl/fl}$ or $Chd4^{\Delta Pax7ER}$ mice at 3 days after muscle injury (n = 4 mice/group). Data were analyzed using gene set enrichment analysis (GSEA) (MySigDB 6.2 Database). Reg, regulation; pol, polymerase. All categories represented obtained $p < 0.0001$.

(B) Color map (coded for Log_2(fold change)) representing targets commonly found to be differentially expressed ($p < 0.01$) in the RNA-seq and protein mass spectrometry of $Chd4^{fl/fl}$ SCs transduced with Ad-CRE or Ad-GFP (n = 4 independent experiments). Data were analyzed using DESeq2 (RNA-seq) or MaxQuant (mass spectrometry).

(C) Genome browser tracks of ATAC-seq data at the *Map1a*, *Ndrg2*, *Myog*, *Tnnt2*, and *Chd5* loci from SCs obtained from TMX-treated $Chd4^{fl/fl}$ and $Chd4^{\Delta Pax7ER}$ mice at 3 days after muscle injury (overlayed tracks of n = 4 mice).

(D) ChIP-qPCR of Chd4 protein binding to the indicated gene loci. The *Tbx21* gene was used as control. Data were normalized to immunoglobulin G (IgG), which was set to 1 (n = 4 independent experiments).

skeletal muscles (Gomez-del Arco et al., 2016). Importantly, chromatin accessibility and chromatin binding assays confirmed that *Map1a*, *Ndrg2*, *Myog*, *Tnnt2*, and *Chd5* are direct CHD4 targets, which explains the loss of their expression in the absence of *Chd4*. *Chd4* depletion also changed the gene expression profiles of the *Chd4* homolog *Chd3* and epigenetic modulators *Ezh2* and *Suz12*. The cross-regulation of *Chd4* and *Chd3* in SCs indicates that several NuRD complexes control SC proliferation, even though the CHD3 and CHD4 proteins form distinct NuRD complexes with specific target genes (Hoffmeister et al., 2017). This functional substitution of CHD4 by either CHD3 or CHD5 may contribute to the observed stem cell lineage-loss phenotype. The biological implication of these changes upon *Chd4* depletion in SCs remains to be determined, despite reports of *Ezh2* controlling SC identity (Juan et al., 2011). The results presented here show that CHD4 exerts a tight control on muscle stem cell fate commitment and lineage fidelity, acting as a master transcriptional repressor of non-muscle lineage genes and of differentiation-specific myogenic genes during the proliferative expansion of SCs. These CHD4-regulated processes are essential for the regenerative functions of muscle stem cells.

EXPERIMENTAL PROCEDURES

Mice

The satellite cell-specific Chd4 transgenic mouse model ($Chd4^{\Delta Pax7ER}$) was generated by crossing mice that express CreERT2 from the Pax7 promoter ($Pax7^{CRE\text{-}ER}$) with Chd4-floxed mice ($Chd4^{fl/fl}$) to generate $Chd4^{\Delta Pax7ER}$ mice. p57 conditional mice were used to generate $Chd4^{\Delta Pax7ER}/p57^{\Delta Pax7ER}$ mice. Genetic ablation was induced by injection of 100 μL of tamoxifen (TMX) (T5648, Sigma-Aldrich, 20 mg/mL in corn oil) intraperitoneally for four consecutive days. $Chd4^{fl/fl}$ mice were used as control for the TMX treatment. Regeneration of skeletal muscle was induced by intramuscular injection of cardiotoxin (CTX; Latoxan, 10^{-5} M). The Catalan Government approved the work protocols, following applicable legislation. Both male and female mice were used in each experiment unless stated otherwise. Live colonies were maintained and genotyped as per Jackson Laboratories' guidelines and protocols. Mice were housed together, health was monitored daily for sickness symptoms, and euthanized immediately at the clinical endpoint when recommended by veterinary and biological services staff members.

SC isolation culture, immunohistochemistry, and cellular assays

A detailed description is provided in supplemental experimental procedures.

RNA-seq and ATAC-seq, ChIP, and RT-qPCR

A detailed description is provided in supplemental experimental procedures.

Statistical analysis

Data were analyzed using GraphPad Prism 8.0. The sample size (n) of each experimental group is described in each corresponding figure legend, and all experiments were repeated at least with three biological replicates. Data presented as mean ± SD. $p < 0.05$ was considered statistically significant. Mann-Whitney U test (independent samples, two sided) was used for pairwise comparisons among groups at each time point.

Data and code availability

RNA-seq and ATAC-seq data have been deposited in the Gene Expression Omnibus (GEO) under accession code GSE179683.

SUPPLEMENTAL INFORMATION

Supplemental information can be found online at https://doi.org/10.1016/j.stemcr.2021.07.022.

AUTHOR CONTRIBUTIONS

Conceptualization, K.S., A.R., J.K., A.L.S., E.P., and P.M.-C.; formal analysis, K.S., A.R., and E.P.; investigation, K.S., A.R., D.M., J.S., I.E., and A.I.; writing –review & editing, K.S., A.R., J.K., A.L.S., E.P., and P.M.-C.; funding acquisition, T.B. and P.M.-C.; resources, F.R., P.G.-d.A., and J.M.R.; visualization, A.L.S. and E. P.; supervision, J.K., A.L.S., E.P., and P.M.-C.

ACKNOWLEDGMENTS

We thank C. Keller for the Pax-CRE-ER mouse line; V. Lukesova, L. Ortet, E. Andrés, and A. Navarro for technical contributions; J. López for bioinformatics; J. Martín-Caballero (PRBB Animal Facilities); O. Fornas (UPF/CRG FACS Facility); A. Dopazo (CNIC-Genomics Facility); E. Rebollo (IBMB-CSIC Molecular Imaging Platform). The authors acknowledge funding from MINECO-Spain (grant no. RTI2018-096068), ERC-AdG-741966, LaCaixa-HEALTH-HR17-00040, MWRF, MDA, UPGRADE-H2020-825825, AFM, and DPP-Spain to P.M.C. P.G.-d.A. was supported by MINECO-Spain (grant no. SAF2016-77816-P); French ANR Labex REVIVE (grant no. ANR-10-LABX-73) to F.R. A.R. was supported by a DCEXS-UPF, BIST Fellowship. Fundació la Marató de TV3 supported A.L.S. (grant no. 202033) and P.M.C. (grant no. 202021) and the María-de-Maeztu-Program for Units of Excellence to UPF (grant no. MDM-2014-0370) and the Severo-Ochoa-Program for Centers of Excellence to CNIC (grant no. SEV-2015-0505).

Received: December 2, 2020
Revised: July 29, 2021
Accepted: July 30, 2021
Published: August 26, 2021

REFERENCES

Egan, C.M., Nyman, U., Skotte, J., Streubel, G., Turner, S., O'Connell, D.J., Rraklli, V., Dolan, M.J., Chadderton, N., Hansen, K., et al. (2013). CHD5 is required for neurogenesis and has a dual role in facilitating gene expression and polycomb gene repression. Dev. Cell *26*, 223–236. https://doi.org/10.1016/j.devcel.2013.07.008.

Ermolaeva, M., Neri, F., Ori, A., and Rudolph, K.L. (2018). Cellular and epigenetic drivers of stem cell ageing. Nat. Rev. Mol. Cell Biol *19*, 594–610. https://doi.org/10.1038/s41580-018-0020-3.

Faralli, H., Wang, C., Nakka, K., Benyoucef, A., Sebastian, S., Zhuang, L., Chu, A., Palii, C.G., Liu, C., Camellato, B., et al. (2016). UTX demethylase activity is required for satellite cell-mediated muscle regeneration. J. Clin. Invest *126*, 1555–1565. https://doi.org/10.1172/JCI83239.

Furumai, R., Matsuyama, A., Kobashi, N., Lee, K.H., Nishiyama, M., Nakajima, H., Tanaka, A., Komatsu, Y., Nishino, N., Yoshida, M., and Horinouchi, S. (2002). FK228 (depsipeptide) as a natural prodrug that inhibits class I histone deacetylases. Cancer Res. *62*, 4916–4921.

Gomez-del Arco, P., Perdiguero, E., Yunes-Leites, P.S., Acin-Perez, R., Zeini, M., Garcia-Gomez, A., Sreenivasan, K., Jimenez-Alcazar, M., Segales, J., Lopez-Maderuelo, D., et al. (2016). The chromatin remodeling complex Chd4/NuRD controls striated muscle identity and metabolic homeostasis. Cell Metab *23*, 881–892. https://doi.org/10.1016/j.cmet.2016.04.008.

Hoffmeister, H., Fuchs, A., Erdel, F., Pinz, S., Grobner-Ferreira, R., Bruckmann, A., Deutzmann, R., Schwartz, U., Maldonado, R., Huber, C., et al. (2017). CHD3 and CHD4 form distinct NuRD complexes with different yet overlapping functionality. Nucleic Acids Res. *45*, 10534–10554. https://doi.org/10.1093/nar/gkx711.

Juan, A.H., Derfoul, A., Feng, X., Ryall, J.G., Dell'Orso, S., Pasut, A., Zare, H., Simone, J.M., Rudnicki, M.A., and Sartorelli, V. (2011). Polycomb EZH2 controls self-renewal and safeguards the transcriptional identity of skeletal muscle stem cells. Genes Dev. *25*, 789–794. https://doi.org/10.1101/gad.2027911.

Kashiwagi, M., Morgan, B.A., and Georgopoulos, K. (2007). The chromatin remodeler Mi-2beta is required for establishment of the basal epidermis and normal differentiation of its progeny. Development *134*, 1571–1582. https://doi.org/10.1242/dev.001750.

Lai, A.Y., and Wade, P.A. (2011). Cancer biology and NuRD: a multifaceted chromatin remodelling complex. Nat. Rev. Cancer *11*, 588–596. https://doi.org/10.1038/nrc3091.

Le Guezennec, X., Vermeulen, M., Brinkman, A.B., Hoeijmakers, W.A., Cohen, A., Lasonder, E., and Stunnenberg, H.G. (2006). MBD2/NuRD and MBD3/NuRD, two distinct complexes with different biochemical and functional properties. Mol. Cell Biol *26*, 843–851. https://doi.org/10.1128/MCB.26.3.843-851.2006.

Mademtzoglou, D., Alonso-Martin, S., Chang, T.H., Bismuth, K., Drayton-Libotte, B., Aurade, F., and Relaix, F. (2017). A p57 conditional mutant allele that allows tracking of p57-expressing cells. Genesis *55*. https://doi.org/10.1002/dvg.23025.

Mademtzoglou, D., Asakura, Y., Borok, M.J., Alonso-Martin, S., Mourikis, P., Kodaka, Y., Mohan, A., Asakura, A., and Relaix, F. (2018). Cellular localization of the cell cycle inhibitor Cdkn1c controls growth arrest of adult skeletal muscle stem cells. eLife *7*. https://doi.org/10.7554/eLife.33337.

Mal, A., Sturniolo, M., Schiltz, R.L., Ghosh, M.K., and Harter, M.L. (2001). A role for histone deacetylase HDAC1 in modulating the transcriptional activity of MyoD: inhibition of the myogenic program. EMBO J. *20*, 1739–1753. https://doi.org/10.1093/emboj/20.7.1739.

Nishijo, K., Hosoyama, T., Bjornson, C.R., Schaffer, B.S., Prajapati, S.I., Bahadur, A.N., Hansen, M.S., Blandford, M.C., McCleish, A.T., Rubin, B.P., et al. (2009). Biomarker system for studying muscle, stem cells, and cancer in vivo. FASEB J. *23*, 2681–2690. https://doi.org/10.1096/fj.08-128116.

O'Shaughnessy, A., and Hendrich, B. (2013). CHD4 in the DNA-damage response and cell cycle progression: not so NuRDy now. Biochem. Soc. Trans. *41*, 777–782. https://doi.org/10.1042/BST20130027.

Ostapcuk, V., Mohn, F., Carl, S.H., Basters, A., Hess, D., Iesmantavicius, V., Lampersberger, L., Flemr, M., Pandey, A., Thoma, N.H., et al. (2018). Activity-dependent neuroprotective protein recruits HP1 and CHD4 to control lineage-specifying genes. Nature *557*, 739–743. https://doi.org/10.1038/s41586-018-0153-8.

Potts, R.C., Zhang, P., Wurster, A.L., Precht, P., Mughal, M.R., Wood, W.H., 3rd, Zhang, Y., Becker, K.G., Mattson, M.P., and Pazin, M.J. (2011). CHD5, a brain-specific paralog of Mi2 chromatin remodeling enzymes, regulates expression of neuronal genes. PLoS One *6*, e24515. https://doi.org/10.1371/journal.pone.0024515.

Robinson, D.C.L., and Dilworth, F.J. (2018). Epigenetic regulation of adult myogenesis. Curr. Top Dev. Biol. *126*, 235–284. https://doi.org/10.1016/bs.ctdb.2017.08.002.

Schworer, S., Becker, F., Feller, C., Baig, A.H., Kober, U., Henze, H., Kraus, J.M., Xin, B., Lechel, A., Lipka, D.B., et al. (2016). Epigenetic stress responses induce muscle stem-cell ageing by Hoxa9 developmental signals. Nature *540*, 428–432. https://doi.org/10.1038/nature20603.

Sreenivasan, K., Ianni, A., Kunne, C., Strilic, B., Gunther, S., Perdiguero, E., Kruger, M., Spuler, S., Offermanns, S., Gomez-del Arco, P., et al. (2020). Attenuated epigenetic suppression of muscle stem cell necroptosis is required for efficient regeneration of dystrophic muscles. Cell Rep *31*, 107652. https://doi.org/10.1016/j.celrep.2020.107652.

Williams, C.J., Naito, T., Arco, P.G., Seavitt, J.R., Cashman, S.M., De Souza, B., Qi, X., Keables, P., Von Andrian, U.H., and Georgopoulos, K. (2004). The chromatin remodeler Mi-2beta is required for CD4 expression and T cell development. Immunity *20*, 719–733. https://doi.org/10.1016/j.immuni.2004.05.005.

Xu, N., Liu, F., Wu, S., Ye, M., Ge, H., Zhang, M., Song, Y., Tong, L., Zhou, J., and Bai, C. (2020). CHD4 mediates proliferation and migration of non-small cell lung cancer via the RhoA/ROCK pathway by regulating PHF5A. BMC Cancer *20*, 262. https://doi.org/10.1186/s12885-020-06762-z.

Yin, H., Price, F., and Rudnicki, M.A. (2013). Satellite cells and the muscle stem cell niche. Physiol. Rev. *93*, 23–67. https://doi.org/10.1152/physrev.00043.2011.

Zhang, P., Wong, C., Liu, D., Finegold, M., Harper, J.W., and Elledge, S.J. (1999). p21(CIP1) and p57(KIP2) control muscle differentiation at the myogenin step. Genes Dev. *13*, 213–224. https://doi.org/10.1101/gad.13.2.213.

Zhang, T., Gunther, S., Looso, M., Kunne, C., Kruger, M., Kim, J., Zhou, Y., and Braun, T. (2015). Prmt5 is a regulator of muscle stem cell expansion in adult mice. Nat. Commun. *6*, 7140. https://doi.org/10.1038/ncomms8140.

Zhang, Y., LeRoy, G., Seelig, H.P., Lane, W.S., and Reinberg, D. (1998). The dermatomyositis-specific autoantigen Mi2 is a component of a complex containing histone deacetylase and nucleosome remodeling activities. Cell *95*, 279–289. https://doi.org/10.1016/s0092-8674(00)81758-4.

Zhao, H., Han, Z., Liu, X., Gu, J., Tang, F., Wei, G., and Jin, Y. (2017). The chromatin remodeler Chd4 maintains embryonic stem cell identity by controlling pluripotency- and differentiation-associated genes. J. Biol. Chem. *292*, 8507–8519. https://doi.org/10.1074/jbc.M116.770248.

Stem Cell Reports, Volume *16*

Supplemental Information

CHD4 ensures stem cell lineage fidelity during skeletal muscle regeneration

Krishnamoorthy Sreenivasan, Alejandra Rodríguez-delaRosa, Johnny Kim, Diana Mesquita, Jessica Segalés, Pablo Gómez-del Arco, Isabel Espejo, Alessandro Ianni, Luciano Di Croce, Frederic Relaix, Juan Miguel Redondo, Thomas Braun, Antonio L. Serrano, Eusebio Perdiguero, and Pura Muñoz-Cánoves

Supplemental information

Chd4 ensures stem cell lineage fidelity during skeletal muscle regeneration

Krishnamoorthy Sreenivasan, Alejandra Rodríguez-delaRosa, Johnny Kim, Diana Mesquita, Jessica Segalés, Pablo Gómez-del Arco, Isabel Espejo, Alessandro Ianni, Luciano Di Croce, Frederic Relaix, Juan Miguel Redondo, Thomas Braun, Antonio L. Serrano, Eusebio Perdiguero, Pura Muñoz-Cánoves

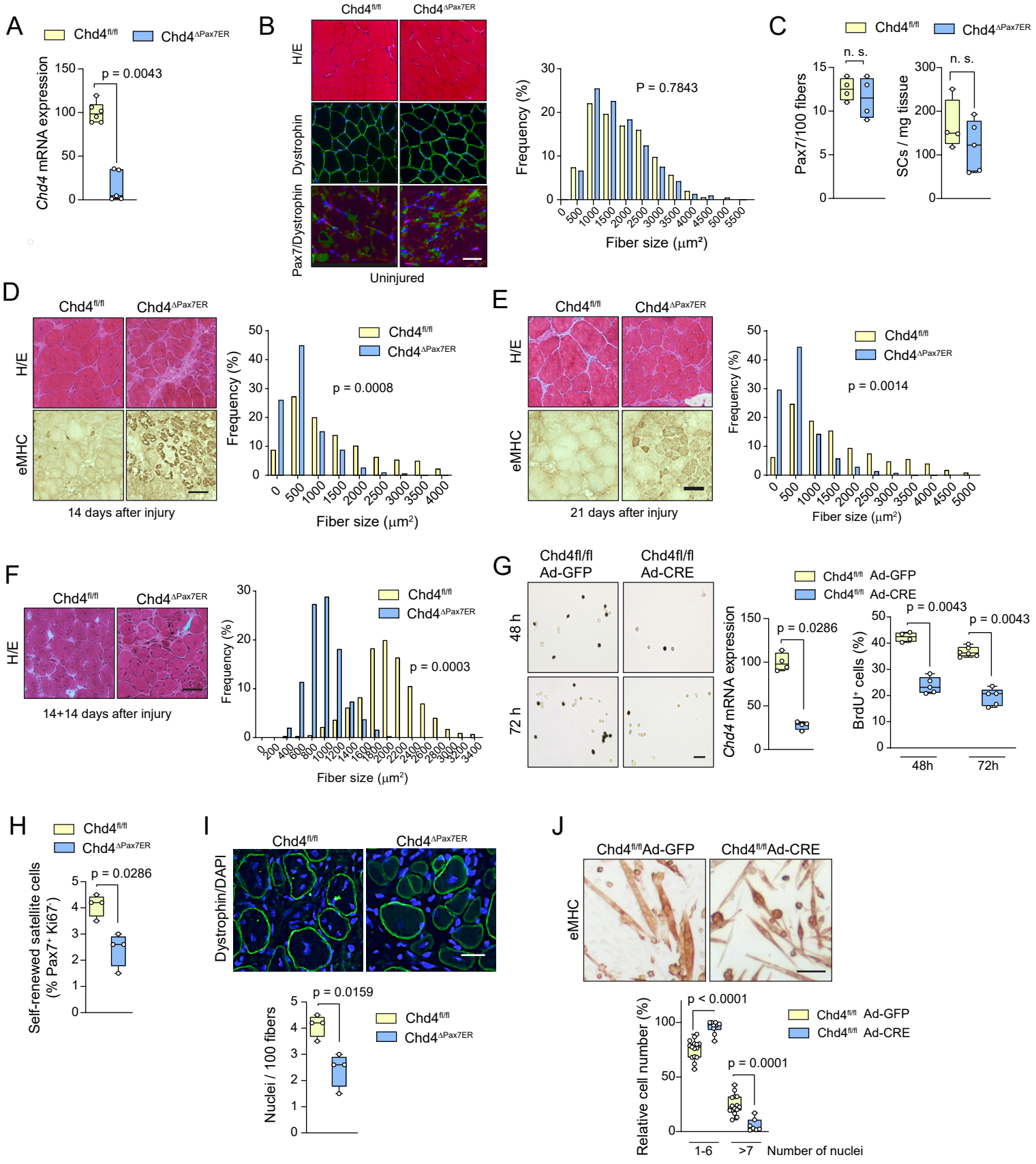
A
Chd4fl/fl
Chd4ΔPax7ER
Chd4 mRNA expression
p = 0.0043
B
H/E
Dystrophin
Pax7/Dystrophin
Uninjured
P = 0.7843
Frequency (%)
Fiber size (μm²)
C
n. s.
Pax7/100 fibers
SCs / mg tissue
D
14 days after injury
p = 0.0008
E
21 days after injury
p = 0.0014
F
14+14 days after injury
p = 0.0003
G
Chd4fl/fl Ad-GFP
Chd4fl/fl Ad-CRE
48 h
72 h
p = 0.0286
p = 0.0043
BrdU+ cells (%)
H
Self-renewed satellite cells (% Pax7+ Ki67-)
I
Dystrophin/DAPI
p = 0.0159
Nuclei / 100 fibers
J
eMHC
p < 0.0001
p = 0.0001
Relative cell number (%)
1-6
>7
Number of nuclei

Figure S1

Figure S1, Related to Figure 1. (A) *Chd4* mRNA expression in FACS-isolated satellite cells from *Chd4* $^{fl/fl}$ or *Chd4* $^{\Delta Pax7ER}$ mice at 30 days after tamoxifen treatment. Data were normalized to the housekeeping gene *Rpl7* (n = 6 or 4 mice, respectively). **(B)** Representative pictures and fiber size distribution of uninjured muscles from tamoxifen-treated *Chd4* $^{fl/fl}$ or *Chd4* $^{\Delta Pax7ER}$ mice (n = 4 mice/group). Scale bar, 50 μm. **(C)** Satellite cell numbers in muscles of *Chd4* $^{fl/fl}$ and *Chd4* $^{\Delta Pax7ER}$ mice at 14 days (left, n = 4 mice/group) and 90 days (right, n = 4 or 5 mice, respectively) after tamoxifen treatment. **(D)** Representative pictures and fiber size distribution of muscles from tamoxifen-treated *Chd4* $^{fl/fl}$ or *Chd4* $^{\Delta Pax7ER}$ mice at 14 days post-injury (n = 3 mice/ group). Scale bar, 50 μm. **(E)** Representative pictures and fiber size distribution of muscles from tamoxifen-treated *Chd4* $^{fl/fl}$and *Chd4* $^{\Delta Pax7ER}$ mice at 21 days post-injury (n = 3 mice/group). Scale bar, 50 μm. **(F)** Representative pictures and fiber size distribution of muscles from tamoxifen-treated *Chd4* $^{fl/fl}$ or *Chd4* $^{\Delta Pax7ER}$ mice at 14 days post-injury (n = 5 or 4 mice, respectively). Scale bar, 50 μm. **(G)** *Chd4* mRNA relative expression and proliferation rate in satellite cells from *Chd4* $^{fl/fl}$ satellite cells transduced with Ad-CRE or Ad-GFP (control) and examined after 48 h (n = 4 or 5 independent experiments, respectively) or 72 h (n = 6 or 5 independent experiments, respectively). Representative pictures of BrdU-stained cells are shown. Scale bar, 50 μm. **(H)** Proportion of quiescent ($Pax7^{+}/Ki67^{-}$) satellite cells in muscles from tamoxifen-treated *Chd4* $^{fl/fl}$ or *Chd4* $^{\Delta Pax7ER}$ mice at 21 dayspost-injury (n = 4 mice/group).
(I) Representative pictures of nuclei and dystrophin staining of muscles from tamoxifen-treated *Chd4* $^{fl/fl}$ or *Chd4* $^{\Delta Pax7ER}$ mice at 7 days post-injury. Quantification of nuclei number inside the myofibers is shown (n = 4 or 5 mice, respectively). Scale bar, 50 μm. **(J)** Representative pictures of cultured myotubes derived from satellite cells of *Chd4* $^{fl/fl}$ mice transduced with Ad-CRE or Ad-GFP (control) and cultured in DM for 48 h. The proportion of myotubes containing the indicated nuclei number is shown. Data were from two independent experiments. Scale bar, 50 μ m.

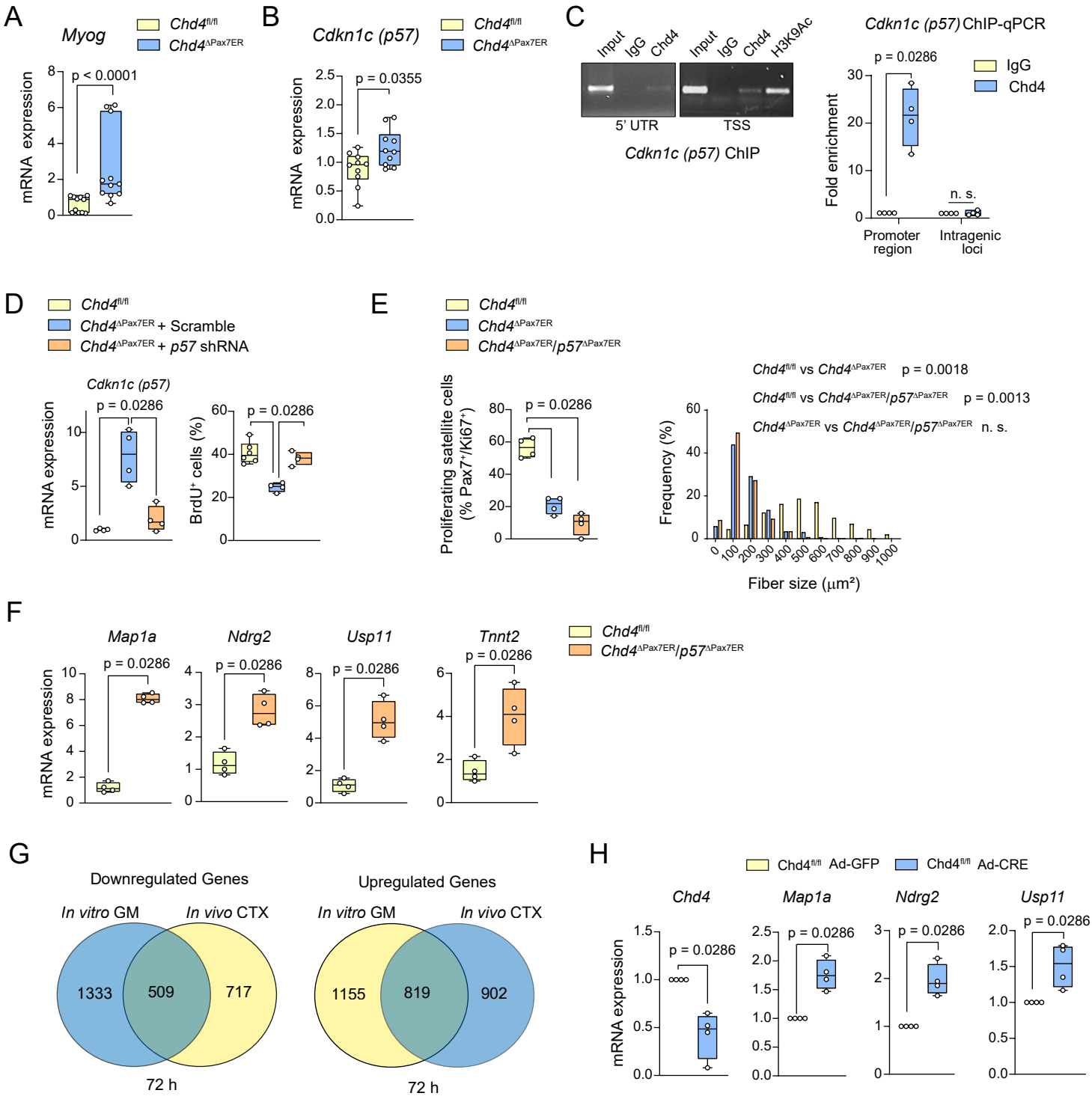
A
Myog
Chd4fl/fl
Chd4ΔPax7ER
mRNA expression
p < 0.0001
B
Cdkn1c (p57)
p = 0.0355
C
Input
IgG
Chd4
H3K9Ac
5' UTR
TSS
Cdkn1c (p57) ChIP
Cdkn1c (p57) ChIP-qPCR
p = 0.0286
n. s.
Fold enrichment
Promoter region
Intragenic loci
D
Chd4ΔPax7ER + Scramble
Chd4ΔPax7ER + p57 shRNA
BrdU+ cells (%)
E
Chd4ΔPax7ER/p57ΔPax7ER
Proliferating satellite cells (% Pax7+/Ki67+)
Chd4fl/fl vs Chd4ΔPax7ER p = 0.0018
Chd4fl/fl vs Chd4ΔPax7ER/p57ΔPax7ER p = 0.0013
Chd4ΔPax7ER vs Chd4ΔPax7ER/p57ΔPax7ER n. s.
Frequency (%)
Fiber size (μm²)
F
Map1a
Ndrg2
Usp11
Tnnt2
G
Downregulated Genes
Upregulated Genes
In vitro GM
In vivo CTX
1333
509
717
1155
819
902
72 h
H
Chd4fl/fl Ad-GFP
Chd4fl/fl Ad-CRE
Chd4
Map1a
Ndrg2
Usp11

Figure S2

Figure S2, Related to Figure 2. (A, B) mRNA expression in FACS-purified satellite cells at 3 days after muscle injury from tamoxifen-treatment of *Chd4* $^{fl/fl}$ or *Chd4*$^{\Delta Pax7ER}$ mice. Data were normalized to the housekeeping gene *Rpl7*, with the *Chd4* $^{fl/fl}$ set to 1 **(**n = 11 mice/group for *Myog*, and n= 10 mice/group for *Cdkn1c*). **(C)** ChIP-PCR analysis of the *Cdkn1c (p57)* promoter region showing binding of the Chd4 protein. Qualitative PCR gel pictures (left) and qPCR analysis (right) are shown. n = 3 samples/group from two biological replicates. **(D)** shRNA-mediated knockdown of *p57* (left) with a lentiviral vector (shRNA p57) in *Chd4*$^{\Delta Pax7ER}$ satellite cells (n= 3 independent experiments); percentage of proliferating satellite cells at 72 h after *p57* silencing as compared to control sRNA-scramble cells, is shown (right) (n = 6, 3, and 3 independent experiments, respectively). **(E)** Quantification of proliferating cells and frequency distribution of cross-sectional area (μm^2) of regenerating fibres from tamoxifen-treated *Chd4* $^{fl/fl}$, *Chd4*$^{\Delta Pax7ER}$ and *Chd4*$^{\Delta Pax7ER}$*/p57*$^{\Delta Pax7ER}$ double-mutant mice at 3 or 7 days post-injury (n= 3 mice/group). **(F)** Relative mRNA expression of the indicated genes in SCs from *Chd4*$^{fl/f}$ or *Chd4*$^{\Delta Pax7ER}$*/p57*$^{\Delta Pax7ER}$ mice at 3 days post-injury (n = 4 mice/group). Data were normalized to the housekeeping gene *Rpl7* with the *Chd4*$^{fl/f}$ set to 1. **(G)** Venn diagram showing the common significantly ($p < 0.01$) upregulated or downregulated genes in the RNA-seq of Ad-CRE or Ad-GFP-treated *Chd4* $^{fl/fl}$ SCs (n = 4 independent experiments), and the RNA-seq of SCs obtained from tamoxifen-treated *Chd4* $^{fl/fl}$ or *Chd4*$^{\Delta Pax7ER}$ mice isolated at 3 days post-injury of muscle (n= 4 mice/group). Data analyzed using DESeq2. **(H)** Relative mRNA expression of the indicated genes in *Chd4*$^{fl/fl}$ SCs transduced with Ad-CRE or Ad-GFP for 48 h. Data were normalized to housekeeping gene *Rpl7* with the Ad-GFP set to 1 (n=4 independent experiments).

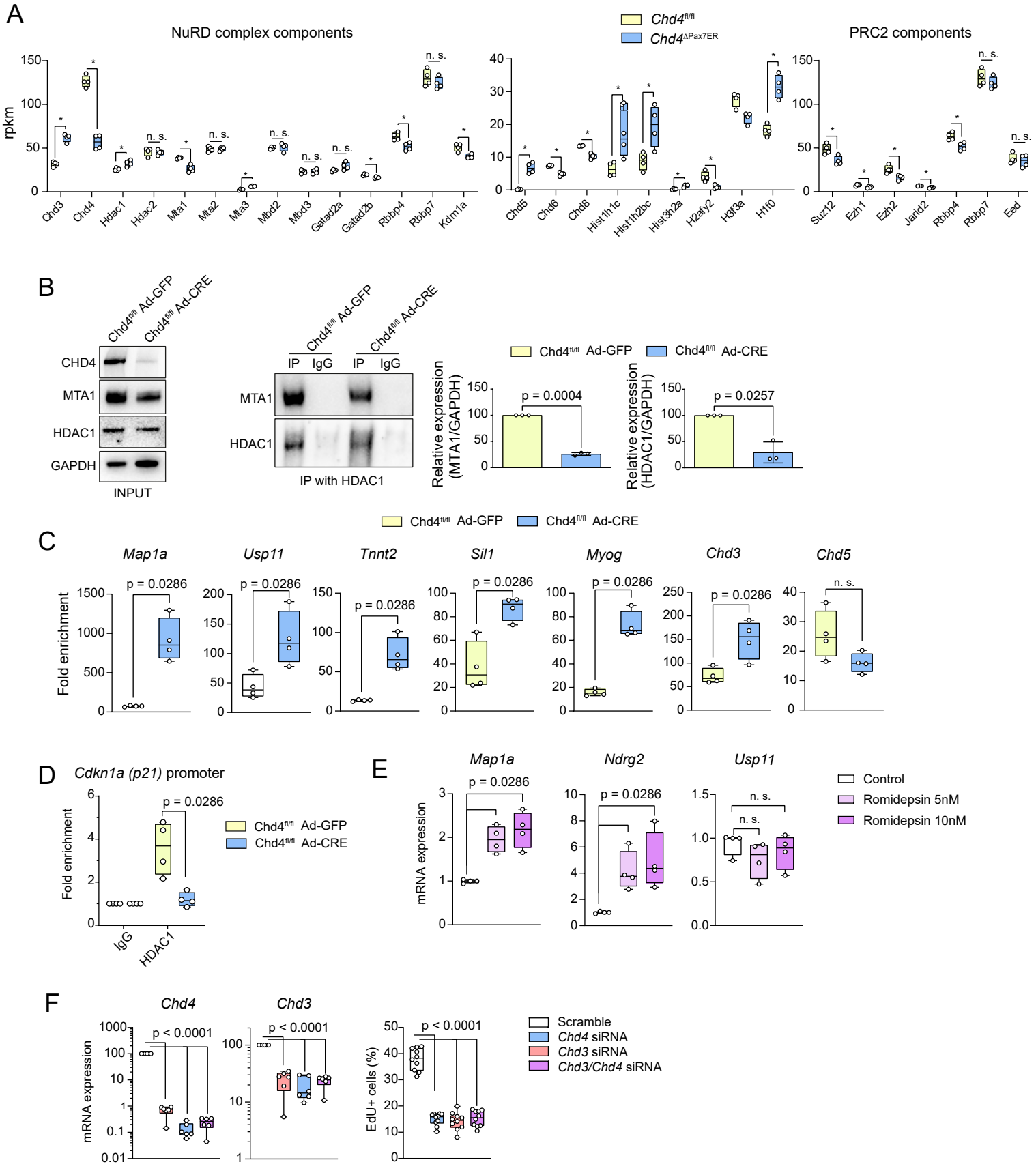
A
NuRD complex components
PRC2 components
Chd4fl/fl
Chd4ΔPax7ER
rpkm
Chd3
Chd4
Hdac1
Hdac2
Mta1
Mta2
Mta3
Mbd2
Mbd3
Gatad2a
Gatad2b
Rbbp4
Rbbp7
Kdm1a
Chd5
Chd6
Chd8
Hist1h1c
Hist1h2bc
Hist3h2a
H2afy2
H3f3a
H1f0
Suz12
Ezh1
Ezh2
Jarid2
Rbbp4
Rbbp7
Eed
n. s.
B
Chd4fl/fl Ad-GFP
Chd4fl/fl Ad-CRE
CHD4
MTA1
HDAC1
GAPDH
INPUT
IP
IgG
IP with HDAC1
Relative expression (MTA1/GAPDH)
Relative expression (HDAC1/GAPDH)
p = 0.0004
p = 0.0257
C
Map1a
Usp11
Tnnt2
Sil1
Myog
Chd3
Chd5
Fold enrichment
p = 0.0286
n. s.
D
Cdkn1a (p21) promoter
IgG
HDAC1
E
Ndrg2
mRNA expression
Control
Romidepsin 5nM
Romidepsin 10nM
F
Chd4
Chd3
p < 0.0001
mRNA expression
EdU+ cells (%)
Scramble
Chd4 siRNA
Chd3 siRNA
Chd3/Chd4 siRNA

Figure S3

Figure S3, Related to Figure 3. (A) Reads per kilobase per million mapped reads (RPKM) of the indicated NuRD complex components, members of the chromodomain helicase DNA-binding (CHD) family, histone variants, and components of the PRC2 complex obtained in the RNA-seq of SCs from tamoxifen-treated *Chd4* $^{fl/fl}$ or *Chd4*$^{\Delta Pax7ER}$ mice, isolated three days post-injury to muscle (n = 4 mice/group). Data were analyzed using DESeq2. (**B**) Western blots of co-immunoprecipitation (IP) experiments showing interactions between MTA1 and HDAC1 in *Chd4*$^{fl/fl}$ SCs transduced with Ad-CRE or Ad-GFP for 48 h. Left, input blots, showing also CHD4 and GAPDH as a control; right, blots of MTA1 and HDAC1 from IP, performed using HDAC1 and IgG antibodies. Quantification of three different experiments is shown. (**C**) ChIP-qPCR of H4 pan-acetyl protein from *Chd4*$^{fl/fl}$ SCs transduced with Ad-CRE or Ad-GFP for 48 h at the indicated genes loci. Data were normalized to IgG (set to 1) (n = 4 independent experiments). (**D**) ChIP-qPCR of HDAC1 protein from *Chd4*$^{fl/fl}$ SCs transduced with Ad-CRE or Ad-GFP for 48 h at the *p21* loci. Data were normalized to IgG (set to 1) (n = 4 independent experiments). (**E**) Effects of HDAC1 inhibition with romidepsin (5 or 10 nM concentrations) in WT SCs on the expression of the indicated genes. Data were normalized to the housekeeping gene *Rpl7*, with the control cells set to 1 (n = 4 independent experiments). (**F**) siRNA-mediated knockdown of *Chd4*, *Chd3*, or both genes using siRNA pools in WT SCs (n = 6 independent experiments). Left, efficiency of the knockdown on *Chd4* and *Chd*3 gene expression; right, percentage of proliferating SCs at 72 h after silencing as compared to control cells (treated with siRNA-scramble).

Supplemental Experimental Procedures

Mice

For mouse experiments, no specific blinding method was used but mice in each sample group were selected randomly.

Isolation of satellite cells by fluorescence-activated cell sorting (FACS)

Dissection of fore and hind limb muscles was done with a scalpel and retrieved in cold DMEM (Dulbecco's Modified Eagle Medium, Gibco). Muscle tissues were finely minced and digested with Liberase 5 mg/mL (Roche/Sigma Aldrich), 0.03% Dispase II (Sigma), DMEM, 1% penicillin/streptomycin, BSA 0.2% (Sigma), 1 M $CaCl_2$, and 1 M $MgCl_2$ at 37ºC. Samples were then centrifuged 10 min at 50*g* at 4ºC. Supernatant was filtered through 100-µm and then a 70-µm cell strainers filters and then centrifuged at 1700 rpm for 15 min. Pellets were then resuspended in Lysis Buffer 1× (BD) and incubated for 10 min. Samples were resuspended in cold DMEM, filtered through 40-µm cell strainer filters, and centrifuged again for 15 min at 1700 rpm. Cells were resuspended in PBS, and 2.5% of goat serum (FACS buffer). Samples were incubated 30 min at 4ºC with the following antibodies: anti-CD45 PE-Cy7 (Biolegend), anti-Sca1 PE-Cy7 (Biolegend), anti-α7-integrin PE (Ablab.ca), and anti-CD34 Alexa-647 (BDPharmingen). Samples were centrifuged at 1700 rpm for 15 min and finally resuspended in FACS buffer with 1 µg/mL DAPI. After antibody labelling, $SCA1^{-}/CD45^{-}/\alpha7\text{-integrin}^{+}/CD34^{+}$ cells were sorted by fluorescence-activated cell sorting (FACS) in the BD Influx cell sorter, and then cultured as described.

Satellite cell culture

Freshly isolated satellite cells from *Pax7*$^{CreERT2/+}$*/Chd4*$^{fl/fl}$ or *Chd4*$^{fl/fl}$ mice were cultured on collagen-coated dishes with HAM's F10 medium (Gibco), 20% Fetal Bovine Serum (FBS), 1:10000 Fibroblast Growth Factor (FGF) and 1% penicillin/streptomycin and kept in an incubator (37ºC, 5% CO_2). *In vitro* genetic ablation of *Chd4* was induced by Adenovirus-Cre 1:2000 transduction during 48 h. Adenovirus-GFP 1:2000 transduction was used as control.

Cell and tissue immunohistochemistry

Tissue samples from tibialis anterior muscles were embedded in optimal cutting temperature (OCT) and frozen in liquid nitrogen-cooled isopentane. Sections (10-µm-thick) were collected and either stained with hematoxylin and eosin (H&E) or immunostained. Freshly isolated or cultured satellite cells were fixed with 4% formaldehyde. Samples were rinsed with PBS, permeabilized with 0.5% Triton X-100 in PBS for 10 min at room temperature, rinsed again with PBS, and then incubated in blocking solution (10% goat serum, 5% BSA) before applying the indicated primary antibodies. For Pax7, Ki67, dystrophin and myogenin immunostainings, samples were incubated for 20 min in 4% PFA, washed with PBS and incubated for 6 min in cold methanol. Sections were then washed with PBS, followed by an antigen retrieval procedure (incubation twice for 5 min at 100 ºC with citric acid 0.1 M pH 6). Afterwards, slides were washed with PBS again and incubated for 2 h in blocking solution (5% BSA IgG-Free with 10% goat serum), followed by a wash with PBS and incubation during 30 min with M.O.M blocking solution (Vector Laboratories). Samples incubated overnight at 4ºC with a primary antibody against Pax7 (sc-81648 Santa Cruz, diluted 1/50 in blocking solution), Ki67 (ab15580, Abcam, diluted 1/100 in blocking solution), dystrophin (Sigma D8168, 1/400), or MyoG (sc-576, Santa Cruz, diluted 1/50). After PBS washing, samples were incubated with the appropriated secondary antibody (Rhodamine Red-X (RRX) AffiniPure Goat Anti-Mouse IgG1, no. 115-295-205; Alexa Fluor 488 AffiniPure Goat AntiRabbit IgG, no. 111-545-144; both from Jackson ImmunoResearch; both were diluted 1/400 in PBS and 1% BSA for use) and rinsed with PBS; nuclei were stained with DAPI (1 µg/mL in PBS) before mounting with Fluoromount (Sigma). For embryonic myosin heavy chain (eMHC) immunostaining, samples were incubated for 30 min with 0.3% H_2O_2, washed with PBS, and incubated 1 h with M.O.M blocking solution (Vector Laboratories). Samples were then incubated with primary anti-eMHC antibody (F1652,

Developmental Studies Hybridoma Bank, undiluted), followed by three PBS washes and incubation with secondary antibody (M.O.M. biotinylated anti-mouse IgG, Vector Laboratories, 1/250 in PBS). Samples were washed with PBS and then incubated with M.O.M ABC solution for 5 min. Slides were then briefly incubated with 3,3'-diaminobenzidine (DAB), and the reaction was stopped by adding H_2O. Slides were dehydrated with ethanol, cleared in xylol, and mounted in di(n-butyl)phthalate in xylene solution (DPX, Sigma-Aldrich). Images were taken using the Zeiss Cell Observer HS widefield microscope with a Zen Blue software, and the image analysis was performed using Fiji image analysis software.

BrdU and EdU incorporation assays

Cultured satellite cells were incubated with BrdU (1.5 µg/mL; Sigma) for 1 h and fixed with formaldehyde 3.7%. Samples were then washed twice with PBS and incubated during 45 min with 1 M HCl at 45ºC, and washed and further incubated for 10 min with 0.1 M borate buffer (7.8 g sodium tetraborate, 4.96 g boric acid, 4L H_2O) at room temperature. Blocking solution (5% donkey serum, 0.5% BSA, 0.25% Triton X-100) was added for 1 h at room temperature. The primary antibody rat anti-BrdU (Ab6326 Abcam, diluted 1/500 in blocking solution) was added and incubated overnight at 4ºC. Samples were then rinsed 3 times with PBS-Tween 0.025% and then incubated with the secondary antibody biotin-Donkey anti-rat (712-066-150 Jackson ImmunoResearch, diluted 1/250 in PBS-Tween 0.025%) for 1 h at room temperature. Samples were washed 3 times with PBS-Tween and then incubated for 30 min with the VECTASTAIN Elite ABC-HRP solution (Vector Labs) at room temperature. Cells were then washed 3 times in PBS-Tween and finally incubated briefly with DAB solution (10 ml PBS, 60 µl DAB 50 µg/ml, 2 µl H_2O_2 30%). The reaction was stopped using distilled water. Samples were stored in PBS and 0.025% sodium azide. EdU incorporation assay was performed with Click-iT™ EdU Cell Proliferation Kit for Imaging (Invitrogen) following manufacturer's instructions. Images were taken using the Zeiss Cell Observer HS widefield microscope with Zen Blue software and the image analysis was performed using Fiji image processing software.

Clonogenic assay

FACS-purified satellite cells were cultured as described in collagen-coated 96 well plates. Total number of cells and colonies were manually counted progressively throughout 4 days.

Time-Lapse Live microscopy

FACS-purified satellite cells were plated in collagen coated µ-Slide Angiogenesis (Ibidi) plates with 1:1 DMEM:HAMs F10 medium containing 20% serum FBS and ITS (Insulin, Transferrin and Selenium; GIBCO) and recorded during 72 h using the Zeiss Cell Observer HS widefield microscope with Zen Blue software. The number of cell divisions and the time for every division was analyzed manually using Fiji image processing software.

RNA isolation

For qPCR and in vitro-based RNA-Seq, total RNA was isolated from cultured satellite cells with the RNeasy Micro kit (QIAGEN) with on-column DNA digestion. For the RNA-Seq experiment in freshly isolated cells, total RNA was extracted with the Arcturus PicoPure RNA Isolation Kit (Thermo Fisher) together with on-column DNA digestion. Both RNA isolation kits were used according to the manufacturer's instructions. RNA concentration was measured with NanoDrop 2000/2000c (Thermo Fisher).

cDNA and qPCR

Reverse transcription of RNA into cDNA was performed by random-primed reverse transcription using the SuperScript II reverse transcriptase (Invitrogen). cDNA quantification was obtained by real-time qPCR (LightCycler 480, Roche) using PowerUp SYBR Green Universal (Thermo Fisher) according to the manufacturer's instructions. Primers used for qPCR are depicted in Supplemental table 1. *Rpl7* transcript levels were used as a reference for the normalization of each target within each sample.

Protein Mass Spectrometry

Whole-cell lysates were run on SDS-PAGE gels and stained with colloidal protein staining solution (Invitrogen). The gels were subjected to digestion with trypsin. Released peptides were measured using LTQ-Orbitrap Velos mass spectrometer (Thermo Fisher Scientific) equipped with a nanoelectrospray source (Proxeon). Raw data from (Sreenivasan et al., 2020) was analyzed using the MaxQuant software package 1.6.1.0.

RNA sequencing

RNA isolation, cDNA, and qPCR are indicated in Supplemental information. RNA integrity and library preparation were checked with a BioAnalyzer (RNA Pico Chip, Agilent). For the in vitro-based RNA-Seq, low input library preparation and single-end sequencing was performed in the Centre de Regulació Genomica (CRG) genomics unit using the HiSeqTM Sequencing Kit and the TruSeq v3 Cluster (Illumina). For the RNA-seq experiment in freshly isolated cells standard Directional RNA-seq library preparation and single-end sequencing (Illumina HiSeq 2500) was performed in the Genomic Unit of Centro Nacional de Investigaciones Cardiovasculares (CNIC). For both datasets RNA-Seq raw reads were assessed for quality, adaptor content and duplication rates with FastQC 0.11.8, trimmed by Cutadapt 1.18 and terminally aligned to the Ensemble mouse genome version mm10 (GRCm38) by HISAT2 2.1.0. Differentially expressed genes were identified using DESeq2 3.6. Only genes with a minimal p-value of 0.01 were classified as significantly differentially expressed. Gene ontology (GO) analysis was performed using Gene Set Enrichment Analysis (GSEA) using MSigDB 6.2 database. Functional annotation clustering was done using DAVID 6.8.

ATAC Sequencing

Library preparation was done on FACS-purified satellite cells following the Omni-ATAC protocol (http://www.nature.com/articles/nmeth.4396). Time of incubation with transposase was set to 40 min after extensive setup with *Chd4* $^{fl/fl}$ satellite cells. Primers used for amplification and sequencing are stated in **Supplemental table 2**. Library quality was assessed by Agilent BioAnalyzer (DNA High Sensitivity Chip). Paired-end sequencing (Illumina HiSeq 2500) was performed in the Genomic Unit of the CRG. Raw reads were assessed for quality, adaptor content and duplication rates with FastQC 0.11.8, trimmed by Cutadapt 1.18 and terminally aligned to the Ensemble mouse genome version mm10 (GRCm38) by Picard 2.18.15. Regions of open chromatin were identified by MACS2 2.1.2 while HOMER was used for peak annotation. Differentially peaks near the Transcriptional Start Site (TSS ± 500 bp) were identified using DESeq2 3.6 ($p < 0.01$). Gene ontology analysis was performed using Gene Set Enrichment Analysis (GSEA) using MSigDB 6.2 database.

ChIP and RT–qPCR

Chromatin immunoprecipitation (ChIP) experiments were performed as previously described (Gomez-del Arco et al., 2016)(Sreenivasan *et al.*, 2020) Chromatin Shearing Kit with SDS (Covaris) was used for chromatin shearing. Briefly, cells were fixed using 1% formaldehyde for 10 minutes and the reaction was quenched with 0.125M glycine for 5 minutes at room temperature. The chromatin were sheared to approximately 300-500bp using Bioruptor (Diagenode). Sheared chromatin was subjected to immunoprecipitation with indicated antibodies. Corresponding mouse or rabbit IgG antibody served as a negative control. Chromatin DNA was verified via quantitative real-time PCR. Primers used in this study are listed in Supplemental Table 1.

Co-immunoprecipitation and western blot analysis

SCs were harvested from *Chd4*$^{fl/fl}$ mice. Genetic ablation of Chd4 was induced *in vitro* by adenoviral transduction with a recombinant adenovirus harboring the Cre recombinase (AdCRE). Control cells were infected with green fluorescent protein (GFP)-expressing virus (AdGFP). Co-immunoprecipitation and western blot analysis was performed as previously described (Ianni et al., 2021), 72 h post-transduction. In this study, anti-HDAC1 antibody (Cell Signaling Technology; 5356) was used for immunoprecipitation and anti-HDAC1 (Cell Signaling Technology; 34589), anti-MTA1

(Cell Signaling Technology; 5647) and anti-CHD4 (Cell Signaling Technology; 12011) antibodies for western blot analysis.

Quantification of Western blot bands and statistical analysis

Intensity of bands was quantified using Image Lab™ software (version 6.0.1; Bio-Rad laboratories) and normalized to loading control (GAPDH). The normalized signal of the control sample for each experiment was set to 100. The abundance of target protein is displayed as fold-change relative to controls (relative expression). Statistical significance was assessed by paired Student's t-test using GraphPad Prism 5.0 Software. *$p<0.05$; ***$p<0.001$.

Data availability

RNA–seq and ATAC-seq data have been deposited in the Gene Expression Omnibus (GEO) under accession code GSE179683. All other data supporting the findings of this study are available from the corresponding author on reasonable request.

Table S1. ChIP and qPCR primers and sequences

Gene	**Forward primer (5′ – 3′)**	**Reverse primer (5′ – 3′)**
Rpl7	GAAGCTCATCTATGAGAAGGC	AAGACGAAGGAGCTGCAGAAC
Chd4	AAGGCCATTGAACGACTGCT	CTCCTCTTCCTCCCCCATCT
p57	CGAGGAGCAGGACGAGAATC	GAAGAAGTCGTTCGCATTGGC
Ndrg2	CAAGGCATGGGCTACATGGC	GGAGAGTCCCAGACTCGCTA
Map1a	GGGGAGAACCTTCAGGTGAC	GACCAGGACGTTCAGTTGCT
Usp11	ATGCGTGATGGACACTATAC	GGCGCTGATAGAACAAGACA
Chd5	TGGACCCTGACTACTGGGAG	CATCCTGCCACTCCTGGTC
Tnnt2	AAGATGCTGAAGAAGGTCCAGTAGA	CACTCTCTCTCCATCGGGG
ChIP qPCR primers		
MyoG	TTATCTGGCTGGGAAGTGGC	GGCAAGGAAGGACAGAGACC
Tnnt2	GACAGTTGGTGGTGGGAGAG	AGCAGGGAGGTAGACCAGAG
Tbx21	CATACAGGAGGCAGCAACAA	TTTCTCTCCCCCAGGAAGTT
Chd5	GGCCCATTGGAGGGGTTATT	ATTTCTCGGGTACCCTCCGT
Chd3	GGGGGTAGAGAGAAGTCGAAAA	GCACCACCCCCAAAAATGTTC
Sil1	TAATAGCCACGCGCCTTCA	CCACCTCCCCTACCTTCGG
Map1a	TCACTTTACCTCCGATCCCAC	CTCAGCATGGCTCAGTTCCA
Ndrg2	TCTTGAGTCATAGCATAGTCATTCT	ACTATTCCTGCTGGAGAACAGC
Usp11	TCCTTTGTGAGGCCCTAAACAC	TCTGCAACCAATACCAGGGG
Cdkn1b	CTAGGTTTCGCGGGCAAAG	AACTAGCCAAACGGCCGGA
p57 promoter	GGTCGAATATGGCCTGAC	CTGAGGAACAATACTGTA
p57 Intragenic	TAACGGCCAGAGAGAACT	TTCTCAATACATTGCACA

Table S2. Primers used for the ATAC-seq, Related to Figure 3

Primer	**Sequence (5′ – 3′)**
Ad1_noMX	AATGATACGGCGACCACCGAGATCTACACTCGTCGGCAGCGTCAGATGTG
Ad2.7	CAAGCAGAAGACGGCATACGAGATGTAGAGAGGTCTCGTGGGCTCGGAGATGT
Ad2.8	CAAGCAGAAGACGGCATACGAGATCCTCTCTGGTCTCGTGGGCTCGGAGATGT
Ad2.9	CAAGCAGAAGACGGCATACGAGATAGCGTAGCGTCTCGTGGGCTCGGAGATGT
Ad2.10	CAAGCAGAAGACGGCATACGAGATCAGCCTCGGTCTCGTGGGCTCGGAGATGT
Ad2.11	CAAGCAGAAGACGGCATACGAGATTGCCTCTTGTCTCGTGGGCTCGGAGATGT
Ad2.12	CAAGCAGAAGACGGCATACGAGATTCCTCTACGTCTCGTGGGCTCGGAGATGT
Ad2.13	CAAGCAGAAGACGGCATACGAGATATCACGACGTCTCGTGGGCTCGGAGATGT
Ad2.14	CAAGCAGAAGACGGCATACGAGATACAGTGGTGTCTCGTGGGCTCGGAGATGT

Ad1_noMX is the common primer for all samples, while the other primers are specific for each of the eight total samples sequenced and act as a barcode.

Supplemental references

Gomez-del Arco, P., Perdiguero, E., Yunes-Leites, P.S., Acin-Perez, R., Zeini, M., Garcia-Gomez, A., Sreenivasan, K., Jimenez-Alcazar, M., Segales, J., Lopez-Maderuelo, D., et al. (2016). The Chromatin Remodeling Complex Chd4/NuRD Controls Striated Muscle Identity and Metabolic Homeostasis. Cell Metab *23*, 881-892. 10.1016/j.cmet.2016.04.008.

Ianni, A., Kumari, P., Tarighi, S., Simonet, N.G., Popescu, D., Guenther, S., Holper, S., Schmidt, A., Smolka, C., Yue, S., et al. (2021). SIRT7-dependent deacetylation of NPM promotes p53 stabilization following UV-induced genotoxic stress. Proc Natl Acad Sci U S A *118*. 10.1073/pnas.2015339118.

Sreenivasan, K., Ianni, A., Kunne, C., Strilic, B., Gunther, S., Perdiguero, E., Kruger, M., Spuler, S., Offermanns, S., Gomez-del Arco, P., et al. (2020). Attenuated Epigenetic Suppression of Muscle Stem Cell Necroptosis Is Required for Efficient Regeneration of Dystrophic Muscles. Cell Rep *31*, 107652. 10.1016/j.celrep.2020.107652.